Advances in the Theory of Brown Dwarfs and Extrasolar Giant Planets

A. Burrows, D. Sudarsky, and C. Sharp

Department of Astronomy and Steward Observatory, University of Arizona, Tucson, AZ 85721

M. Marley

Department of Astronomy, New Mexico State University, Box 30001/Dept. 4500, Las Cruces NM 88003

W.B. Hubbard and J.I. Lunine

Lunar and Planetary Laboratory, University of Arizona, Tucson, AZ 85721

T. Guillot

Department of Meteorology, University of Reading, P.O. Box 239, Whiteknights, Reading RG6 6AU, United Kingdom

D. Saumon

Department of Physics and Astronomy, Vanderbilt University, Nashville, TN 37235

R. Freedman

Space Physics Research Institute, NASA Ames Research Center, Moffett Field CA 94035

Abstract.

We have developed a new non–gray theory of the evolution, spectra, and colors of extrasolar giant planets (EGPs) and brown dwarfs that reveals their exotic nature and uniqueness. We have discovered that the fluxes of such objects for $T_{\rm eff}$s from 1300 K to 100 K can be spectacularly higher in the near infrared bands than black body values and that their infrared colors are quite blue. As a consequence, EGPs and brown dwarfs reside in hitherto unoccupied realms of the H–R diagram and may be more easily found with current and planned telescopes than previously imagined.

1. Introduction

Doppler spectroscopy has now revealed about 20 objects in the giant planet/brown dwarf regime, including companions to τ Boo, 51 Peg, υ And, 55 Cnc, ρ CrB, 70 Vir, 16 Cyg, and 47 UMa (Butler *et al.* 1997; Cochran *et al.* 1997; Marcy

& Butler 1996; Butler & Marcy 1996; Mayor & Queloz 1995; Latham *et al.* 1989). Furthermore, the brown dwarf, Gl229B, has been discovered (Oppenheimer *et al.* 1995; Nakajima *et al.* 1995; Matthews *et al.* 1996; Geballe *et al.* 1996). Gl229B is a milestone because it displays methane spectral features and low surface fluxes that are unique to objects with effective temperatures (in this case, $T_{\rm eff}\sim$950 K) below the solar–metallicity main sequence edge. In 1995 and 1996, we published a gray theory of the evolution of extrasolar giant planets (EGPs) with masses from 0.3 $M_{\rm J}$ to 15 $M_{\rm J}$, where $M_{\rm J}$ denotes a Jupiter mass ($\sim$0.001 $M_\odot$) (Burrows *et al.* 1995; Saumon *et al.* 1996; Guillot *et al.* 1996).

We (Burrows *et al.* 1997) have now developed a *non–gray* theory that encompasses the EGP/brown dwarf domains from 0.3 $M_{\rm J}$ to 70 $M_{\rm J}$, in aid of the direct searches for substellar objects, be they "planets" or brown dwarfs, being planned (TOPS and ExNPS reports; Leger *et al.* 1993). We have limited themselves to *solar–metallicity* objects in isolation and ignored the effects of stellar insolation (Guillot *et al.* 1996). In this communication, we summarize some of the results of this extensive new study, to which we refer the reader for details.

2. Modeling Technique

The opacities we employed are from extensions of the HITRAN database (Rothman *et al.* 1992, 1997), the GEISA database (Husson *et al.* 1997), and theoretical calculations (Tyuterev *et al.* 1994; Goorvitch 1994; Tipping 1990; Wattson & Rothman 1992; L. R. Brown, private communication). For water, we used the new Partridge & Schwenke H_2O database. Our line list includes 1.9×10^6 lines for CH_4 and CH_3D, 99,000 lines for CO, 11,400 lines for NH_3, 11,240 lines for PH_3, and 179,000 lines for H_2S. Modeled continuum opacity sources include H^- and H_2^- opacity and collision–induced absorption (CIA) of H_2 and helium (Borysow & Frommhold 1990; Zheng & Borysow 1995). The latter is a direct function of pressure and a major process in EGP/brown dwarf atmospheres.

To calculate atmosphere profiles and spectra, we used the k–coefficient method (Goody *et al.* 1989; Lacis & Oinas 1991), widely used in planetary atmosphere modeling (see M. Marley, this volume). This is not the ODF technique (Saxner & Gustafsson 1984) and gives excellent agreement with full line–by–line computations of atmospheric transmission (Grossman & Grant 1992,1994a,1994b).

Chemical equilibrium calculations were performed with the ATLAS code and data from Kurucz (1970). The Kurucz reaction constants are inaccurate at low temperatures, but the $NH_3\rightarrow N_2$ and $CH_4\rightarrow$ CO conversions that occur in EGPs and brown dwarfs do so in regions of $T-P$ space for which the Kurucz reaction constants are accurate. Condensation of NH_3, H_2O, Fe, and $MgSiO_3$ was included using data from various sources, including Eisenberg & Kauzmann (1969), the Handbook of Chemistry and Physics (1993), and Lange's Handbook of Chemistry (1979). Following Fegley & Lodders (1994, 1996), we assumed that Al, Ca, Ti and V were removed either by condensation or were dissolved in silicate grains at about the $MgSiO_3$ condensation temperature.

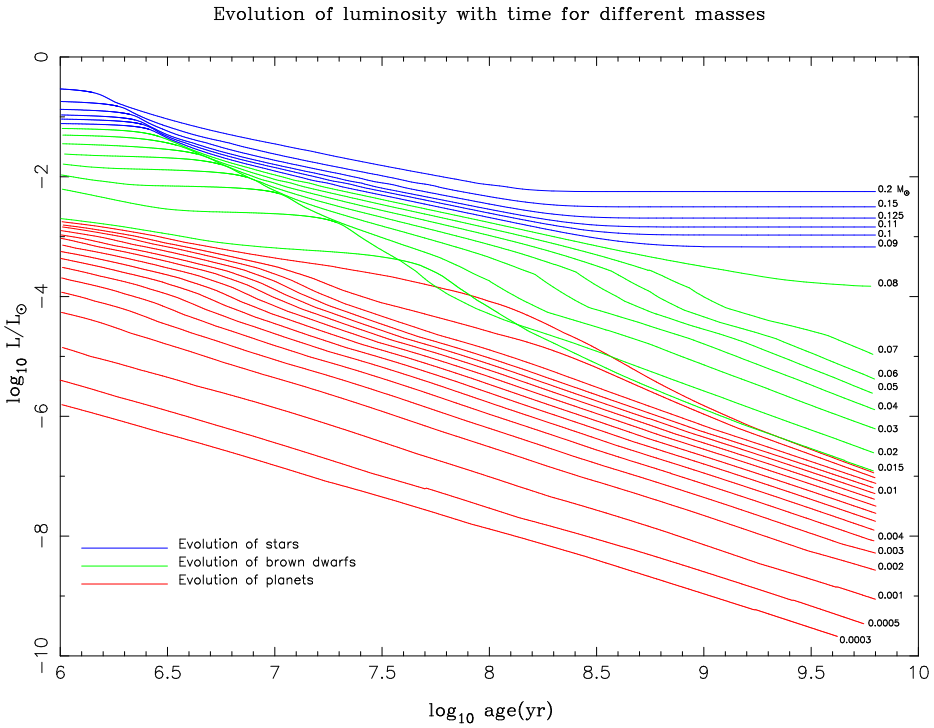

Figure 1. Evolution of the luminosity (in $L_\odot$) of solar–metallicity M dwarfs and substellar objects versus time (in years) after formation. The stars, "brown dwarfs" and "planets" are shown as solid, dashed, and dot–dashed curves, respectively. In this figure, we arbitrarily designate as "brown dwarfs" those objects that burn deuterium, while we designate those that do not as "planets." The masses in $M_\odot$ label most of the curves, with the lowest three corresponding to the mass of Saturn, half the mass of Jupiter, and the mass of Jupiter.

3. Evolutionary Models

In Burrows *et al.* (1995) and Saumon *et al.* (1996), we published cooling curves for EGPs and small brown dwarfs that were based upon our then–current atmosphere models. In Burrows *et al.* (1997), we have updated the H_2 CIA, H_2O, and CH_4 opacities and the radiative transfer algorithm, as well as the chemical equilibrium calculations. Consequently, the evolutionary tracks have changed, but generally by no more than 10% in luminosity at any given time, for any given mass.

Figure 1 depicts the updated luminosity versus time plots for objects from Saturn's mass (0.3 $M_{\rm J}$) to 0.2 $M_\odot$. It covers three orders of magnitude in mass and encapsulates the characteristics of the entire family of substellar objects and the transition to stars.

Tables 1–3 summarize the evolution of various structural parameters versus time for EGP masses of 4 $M_{\rm J}$, 15 $M_{\rm J}$, and 20 $M_{\rm J}$.

The early plateaux in Figure 1 between 10^6 years and 10^8 years are due to deuterium burning, where the initial deuterium mass fraction was taken to be

Table 1. Evolution of planet/brown dwarf of mass = 4 Jupiter masses

$\log t$ (Gyr)	$T_{\rm eff}$ (K)	$\log L/L_\odot$	R (10^9 cm)	$\log T_c$ (K)	$\log \rho_c$ (g cm^{-3})	$L_{\rm nuclear}/L$
−2.998	1652.0	−3.666	12.46	5.132	0.561	0.000
−2.794	1510.0	−3.877	11.72	5.127	0.627	0.000
−2.592	1353.0	−4.112	11.12	5.118	0.685	0.000
−2.385	1237.0	−4.310	10.59	5.104	0.740	0.000
−2.183	1112.0	−4.533	10.14	5.085	0.792	0.000
−1.976	981.9	−4.783	9.75	5.061	0.840	0.000
−1.768	860.4	−5.042	9.44	5.034	0.881	0.000
−1.558	748.9	−5.308	9.17	5.004	0.918	0.000
−1.346	648.5	−5.579	8.94	4.974	0.949	0.000
−1.136	562.7	−5.845	8.75	4.944	0.977	0.000
−0.927	490.3	−6.100	8.59	4.914	1.000	0.000
−0.715	427.3	−6.354	8.44	4.884	1.022	0.000
−0.503	373.3	−6.603	8.30	4.852	1.041	0.000
−0.303	328.7	−6.836	8.19	4.822	1.058	0.000
−0.100	288.5	−7.074	8.08	4.790	1.074	0.000
0.103	253.0	−7.313	7.98	4.757	1.088	0.000
0.306	222.2	−7.548	7.89	4.724	1.102	0.000
0.507	196.8	−7.769	7.81	4.691	1.114	0.000
0.709	176.2	−7.969	7.73	4.654	1.126	0.000
0.912	158.2	−8.166	7.65	4.613	1.138	0.000

Table 2. Evolution of planet/brown dwarf of mass = 15 Jupiter masses

$\log t$ (Gyr)	$T_{\rm eff}$ (K)	$\log L/L_\odot$	R (10^9 cm)	$\log T_c$ (K)	$\log \rho_c$ (g cm^{-3})	$L_{\rm nuclear}/L$
−2.993	2522.0	−2.701	16.24	5.609	0.840	0.020
−2.777	2484.0	−2.793	15.07	5.624	0.932	0.054
−2.565	2431.0	−2.902	13.88	5.638	1.036	0.155
−2.348	2369.0	−3.017	12.80	5.648	1.139	0.385
−2.129	2311.0	−3.114	12.04	5.653	1.217	0.680
−1.916	2264.0	−3.181	11.61	5.654	1.264	0.851
−1.713	2220.0	−3.239	11.30	5.653	1.299	0.881
−1.512	2143.0	−3.333	10.87	5.651	1.349	0.843
−1.310	1956.0	−3.545	10.23	5.644	1.428	0.744
−1.109	1621.0	−3.940	9.45	5.623	1.533	0.544
−0.904	1325.0	−4.354	8.77	5.586	1.630	0.262
−0.704	1095.0	−4.739	8.25	5.536	1.710	0.108
−0.503	890.3	−5.136	7.91	5.487	1.765	0.054
−0.301	740.3	−5.481	7.68	5.442	1.801	0.030
−0.099	628.2	−5.785	7.52	5.401	1.829	0.017
0.115	526.9	−6.106	7.39	5.361	1.851	0.010
0.328	450.7	−6.390	7.28	5.325	1.869	0.006
0.536	390.6	−6.649	7.20	5.290	1.884	0.004
0.740	339.9	−6.900	7.12	5.255	1.897	0.002
0.946	295.7	−7.150	7.05	5.221	1.909	0.001

Table 3. Evolution of planet/brown dwarf of mass = 20 Jupiter masses

$\log t$ (Gyr)	$T_{\rm eff}$ (K)	$\log L/L_\odot$	R (10^9 cm)	$\log T_c$ (K)	$\log \rho_c$ (g cm^{-3})	$L_{\rm nuclear}/L$
−2.988	2674.0	−2.251	24.27	5.619	0.489	0.005
−2.779	2668.0	−2.394	20.68	5.664	0.678	0.052
−2.563	2642.0	−2.532	18.00	5.701	0.848	0.392
−2.344	2627.0	−2.597	16.88	5.718	0.928	0.877
−2.137	2620.0	−2.620	16.52	5.723	0.955	0.933
−1.933	2609.0	−2.657	15.97	5.731	0.998	0.895
−1.733	2564.0	−2.770	14.53	5.752	1.119	0.660
−1.530	2313.0	−3.201	10.88	5.785	1.493	0.000
−1.328	1871.0	−3.709	9.25	5.762	1.704	0.000
−1.123	1525.0	−4.127	8.62	5.733	1.797	0.000
−0.923	1325.0	−4.412	8.21	5.701	1.860	0.000
−0.721	1168.0	−4.668	7.88	5.665	1.913	0.000
−0.509	1002.0	−4.965	7.61	5.624	1.958	0.000
−0.307	856.9	−5.258	7.41	5.585	1.992	0.000
−0.097	734.7	−5.545	7.25	5.546	2.020	0.000
0.118	621.0	−5.853	7.12	5.506	2.043	0.000
0.331	527.6	−6.148	7.02	5.471	2.061	0.000
0.539	456.9	−6.408	6.94	5.437	2.076	0.000
0.740	400.2	−6.648	6.87	5.405	2.089	0.000
0.949	348.8	−6.895	6.80	5.371	2.101	0.000

2×10^{-5}. Deuterium burning occurs earlier, is quicker, and is at higher luminosity for the more massive models, but can take as long as 10^8 years for a 15 $M_{\rm J}$ object. The mass below which less than 50% of the "primordial" deuterium is burnt is $\sim$13 $M_{\rm J}$ (Burrows *et al.* 1995). On this figure, we have arbitrarily classed as "planets" those objects that do not burn deuterium and as "brown dwarfs" those that do burn deuterium, but not light hydrogen. While this distinction is physically motivated, we do not advocate abandoning the definition based on origin. Nevertheless, the separation into M dwarfs, "brown dwarfs", and giant "planets" is useful for parsing by eye the information in the figure.

In Figure 1, the bumps between 10^{-4} $L_\odot$ and 10^{-3} $L_\odot$ and between 10^8 and 10^9 years, seen on the cooling curves of objects from 0.03 $M_\odot$to 0.08 $M_\odot$, are due to silicate and iron grain formation. These effects, first pointed out by Lunine *et al.* (1989), occur for $T_{\rm eff}$s between 2500 K and 1300 K. Since grain and cloud models are problematic, there still remains much to learn concerning their role and how to model them (see F. Allard, this volume).

Bolometric luminosity and age can be used to yield mass and radius. Effective temperature and mass can provide age and luminosity. Fits to the UKIRT spectrum of Gl229B (Marley *et al.* 1996; Allard *et al.* 1996; Tsuji *et al.* 1996) give $T_{\rm eff}\sim$900–1000 K and g$\sim10^{5\pm0.5}$ cm s^{-2}. One obtains a mass between 15 $M_{\rm J}$ and 60 $M_{\rm J}$, with a best value near 35 $M_{\rm J}$, and an age between $10^{8.5}$ and $10^{9.5}$ years. The wide range in inferred Gl229B parameters is a direct consequence of the weakness of our current constraints on gravity.

3.1. Metallicity Dependence

Recently, we have completed a set of evolutionary models that explore the characteristics of the edge of the main sequence as a function of metallicity and atmosphere model (Saumon *et al.* 1997, in preparation). As a part of this effort, we generated 10^{10}–year isochrones for models with metallicities of solar,

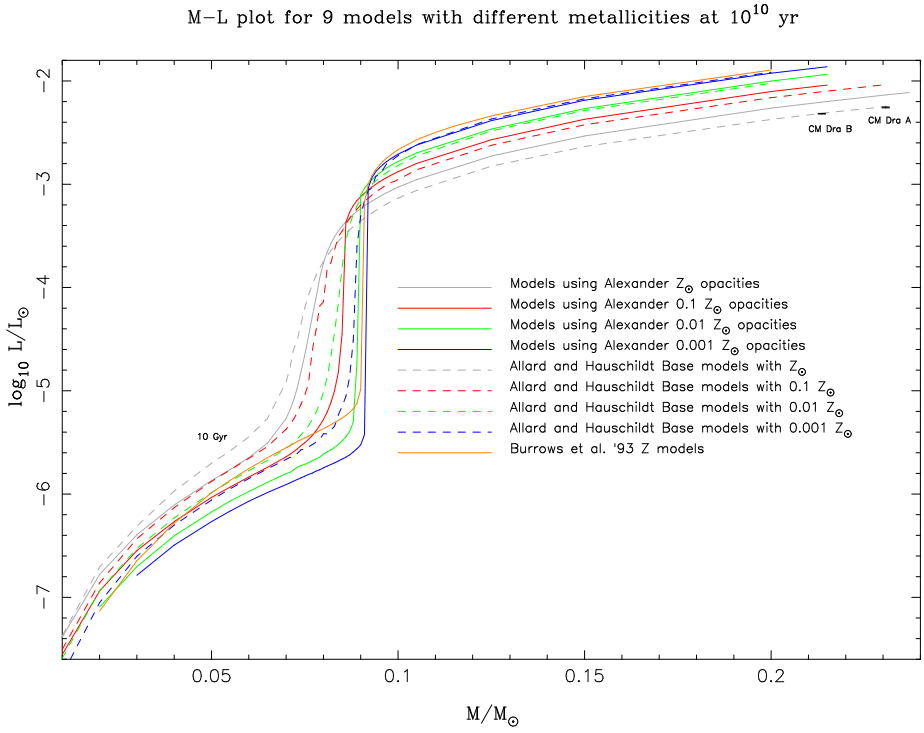

Figure 2. Luminosity (in $L_\odot$) versus mass (in solar masses) for a variety of atmosphere models and metallicities, at an age of 10^{10} years. We performed all of the evolutionary calculations using our own codes and approaches, but employed the atmosphere models of Allard & Hauschildt (1995), Alexander (1996), Burrows *et al.* (1993), and Saumon *et al.* (1994). Systematically, the luminosity of an M dwarf is higher, and that of a brown dwarf is lower, for lower metallicities.

0.1×solar, 0.01×solar, 0.001×solar, and zero (Saumon *et al.* 1994), employing atmosphere models of our own manufacture, as well as those from Alexander (1996) and Allard & Hauschildt (1995). Figure 2 depicts the nature of the transition from brown dwarfs to M dwarfs for this range of metallicities.

We display these numerical data to caution the reader that the metallicity dependence is systematic and non–trivial. Figure 2 demonstrates clearly that the mass/luminosity slope at the boundary is a strong function of $\log_{10}$Z. In particular, the metallicity dependence will be a factor in the proper conversion of luminosity functions into mass functions for objects in the field, in open clusters, and in globular clusters.

4. EGP and Brown Dwarf Spectra

There are a few major aspects of EGP/brown dwarf atmospheres that bear listing and that uniquely characterize them. Below $T_{\rm eff}$s of 1200 K, the dominant equilibrium carbon molecule is CH_4, not CO, and below 600 K the dominant nitrogen molecule is NH_3, not N_2. The major opacity sources are H_2, H_2O,

CH_4, and NH_3. For $T_{\rm eff}$s below $\sim$400 K, water clouds form at or above the photosphere and for $T_{\rm eff}$s below 200 K, ammonia clouds form (*viz.,* Jupiter). Collision–induced absorption of H_2 partially suppresses emissions longward of $\sim$10 μm. The holes in the opacity spectrum of H_2O that define the classic telluric IR bands also regulate much of the emission from EGP/brown dwarfs in the near infrared. Importantly, the windows in H_2O and the suppression by H_2 conspire to force flux to the blue for a given $T_{\rm eff}$. The upshot is an exotic spectrum enhanced relative to the black body value in the J and H bands ($\sim$1.2 μm and $\sim$1.6 μm, respectively) by as much as *two* to *ten* orders of magnitude, depending upon $T_{\rm eff}$. In addition, as $T_{\rm eff}$ decreases below $\sim$1000 K, the flux in the M band ($\sim$5 μm) is progressively enhanced relative to the black body value. While at 1000 K there is no enhancement, at 200 K it is near 10^5. Hence, the J, H, and M bands are the premier bands in which to search for cold substellar objects. Eventhough K band ($\sim$2.2 μm) fluxes are generally higher than black body values, H_2 and CH_4 absorption features in the K band decrease its importance *relative* to J and H. As a consequence of the increase of atmospheric pressure with decreasing $T_{\rm eff}$, the anomalously blue $J-K$ and $H-K$ colors get *bluer*, not redder.

Note that the presence or absence of clouds strongly affects the reflection albedos of EGPs and brown dwarfs. In particular, when there are clouds at or above the photosphere, the albedo in the optical is high. Conversely, when clouds are absent, the albedo in the mostly absorbing atmosphere is low. Recall, however, that in Burrows *et al.* (1997) we ignored reflection effects.

Figure 3 depicts the object's surface flux versus wavelength for representative $T_{\rm eff}$s from 130 K to 1000 K at a gravity of 3.0×10^4 cm s^{-2}.

The corresponding masses range from $\sim$13 $M_{\rm J}$ to $\sim$16 $M_{\rm J}$ and the corresponding ages range from 0.25 Gyrs to 7 Gyrs. Superposed on Figure 3 are the positions of various prominent molecular bands and the J, H, K, and M bands. As is clear from the figure, H_2O defines much of the spectrum, but CH_4 and H_2 modify it in useful ways. CH_4 absorption features near 1.65 μm, 2.2 μm, and 3.3 μm are particularly relevant, the latter two decreasing the K and L' ($\sim$3.5 μm) band fluxes, respectively. NH_3 near 6 μm becomes important below 250 K and the CH_4 feature around 7.8 μm deepens with decreasing $T_{\rm eff}$. However, it should be noted that in Jupiter the 7.8 μm absorption feature is inverted into a stratospheric emission feature. Since a stratosphere requires UV flux from the primary or another energy deposition mechanism, our models do not address this possibility. In addition, we find that H_2O and NH_3 features near 6 μm make the band from 5.5 to 7 μm less useful for searching for brown dwarfs and EGPs.

Figure 4 depicts spectra between 1 μm and 40 μm at a detector 10 parsecs away from objects with age 1 Gyr and masses from 1 $M_{\rm J}$ through 40 $M_{\rm J}$. Superposed are the corresponding black body curves and the putative sensitivities for the three NICMOS cameras (Thompson 1992), ISO (Benvenuti *et al.* 1994), SIRTF (Erickson & Werner 1992), and Gemini/SOFIA (Mountain *et al.* 1992; Erickson 1992). Figure 4 demonstrates how unlike a black body an EGP spectrum is. Note on Figure 4 the H_2–induced suppression at long wavelengths and the enhancement at shorter wavelengths. For example, the enhancement at 5 μm for a 1 Gyr old, 1 $M_{\rm J}$ extrasolar planet is by four o rders of magnitude.

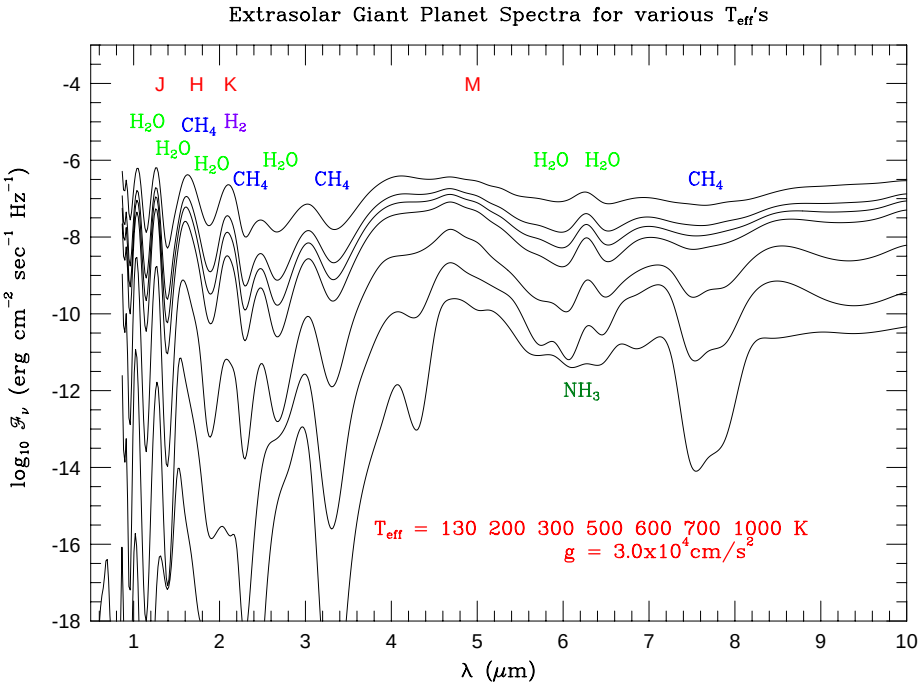

Figure 3. Surface flux (in erg cm^{-2} sec^{-1} Hz^{-1}) versus wavelength (in microns) from 1 μm to 10 μm for $T_{\rm eff}$s of 130, 200, 300, 500, 600, 700, and 1000 K, at a surface gravity of 3.0×10^4 cm s^{-2}. Shown are the positions of the J, H, K, and M bands and various molecular absorption features.

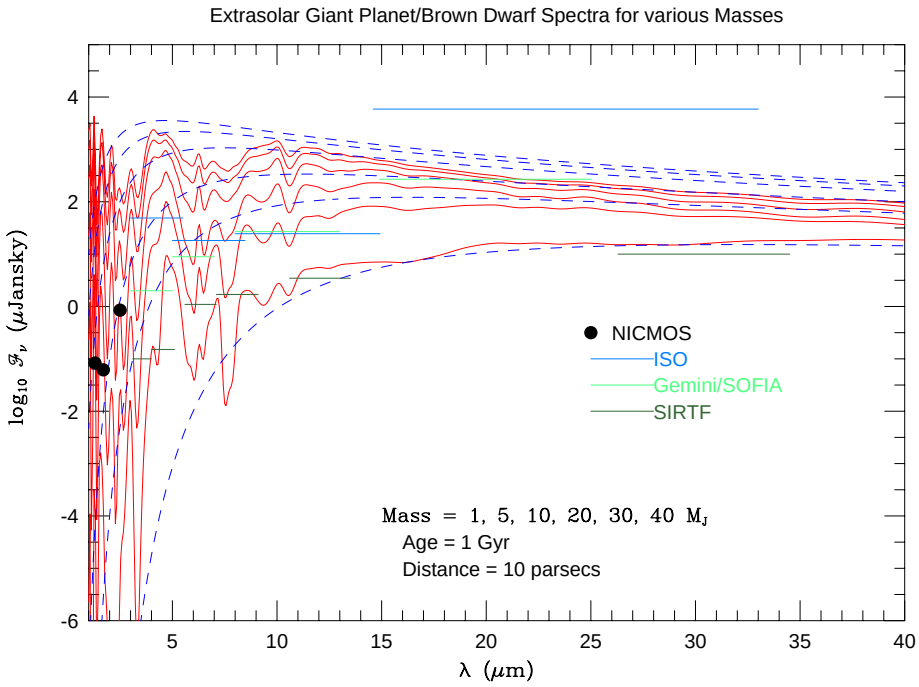

Figure 4. The flux (in μJanskys) at 10 parsecs versus wavelength (in microns) from 1 μm to 40 μm for 1, 5, 10, 20, 30, and 40 M_J models at 1 Gyr. Superposed for comparison are the corresponding black body curves (dashed) and the putative sensitivities of the three NICMOS cameras, ISO, Gemini/SOFIA, and SIRTF. NICMOS is denote with large black dots, ISO with thin, dark lines, Gemini/SOFIA with thin, light lines, and SIRTF with thicker, dark lines. At all wavelengths, SIRTF's projected sensitivity is greater than ISO's. SOFIA's sensitivity overlaps with that of ISO around 10 μm. For other wavelength intervals, the order of sensitivity is SIRTF > Gemini/SOFIA > ISO, where > means "is more sensitive than." Note the suppression relative to the black body values at the longer wavelengths.

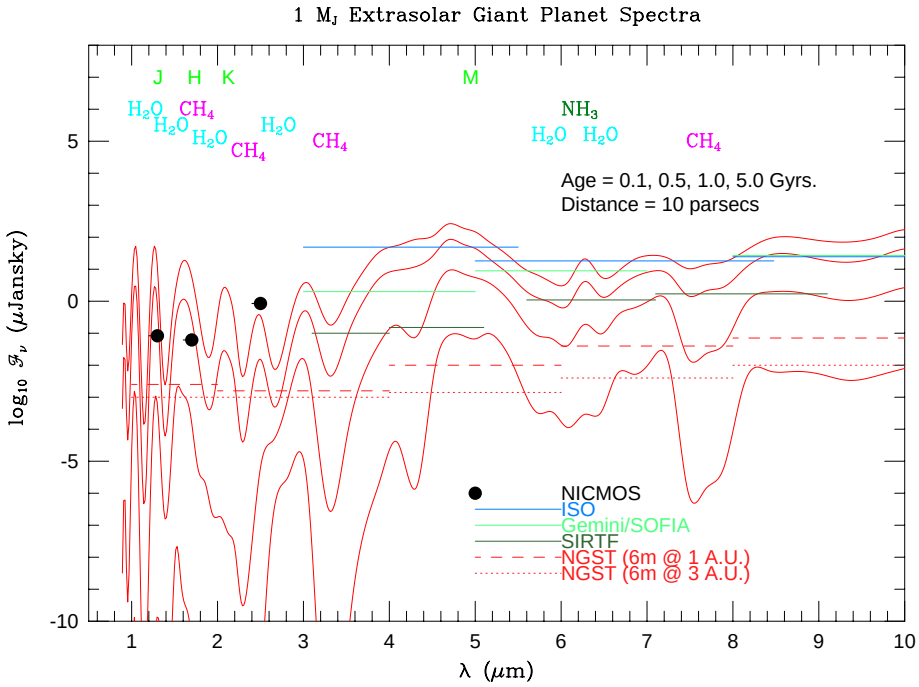

Figure 5. The flux (in μJanskys) at 10 parsecs versus wavelength (in microns) from 1 μm to 10 μm for a 1 $M_{\rm J}$ object at ages of 0.1, 0.5, 1.0, and 5.0 Gyr. Superposed are the positions of the J, H, K, and M bands, as well as the estimated sensitivities of the three NICMOS cameras, ISO, Gemini/SOFIA, SIRTF, and NGST.

Comparison with the sensitivities reveals that the range for detection by SIRTF at 5 μm of a 1 Gyr old, 1 $M_{\rm J}$ object in isolation is near 100 parsecs. The range for NICMOS in H for a 1 Gyr old, 5 $M_{\rm J}$ object is approximately 300 parsecs, while for a coeval 40 $M_{\rm J}$ object it is near 1000 parsecs. These are dramatic numbers that serve to illustrate both the promise of the new detectors and the enhancements we theoretically predict.

Figures 5–7 portray the evolution from 0.1 Gyr to 5 Gyr of the spectra from 1 μm to 10 μm of objects with masses of 1, 5, and 25 $M_{\rm J}$. The higher curves are for the younger ages. These cooling curves summarize EGP/brown dwarf spectra and their evolution. Figure 7 suggests that SIRTF will be able to see at 5 μm a 5 Gyr old, 25 $M_{\rm J}$ object in isolation out to $\sim$500 parsecs and that NICMOS will be able to see at J or H a 0.1 Gyr old object with the same mass out to $\sim$3000 parsecs. Note that the J and H flux enhancements over black body values for the 1 $M_{\rm J}$ model after 0.1 Gyr are at least ten orders of magnitude. However, it must be remembered that these models do not include a reflected light component from a primary.

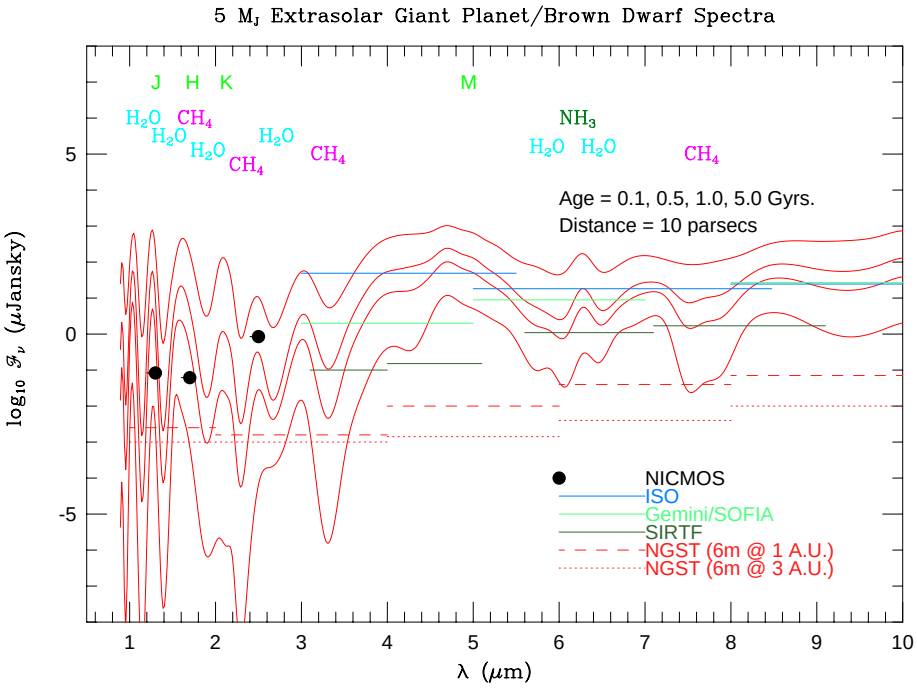

Figure 6. The flux (in μJanskys) at 10 parsecs versus wavelength (in microns) from 1 μm to 10 μm for a 5 $M_{\rm J}$ object at ages of 0.1, 0.5, 1.0, and 5.0 Gyr. Superposed are the positions of the J, H, K, and M bands, as well as the estimated sensitivities of the three NICMOS cameras, ISO, Gemini/SOFIA, SIRTF, and NGST.

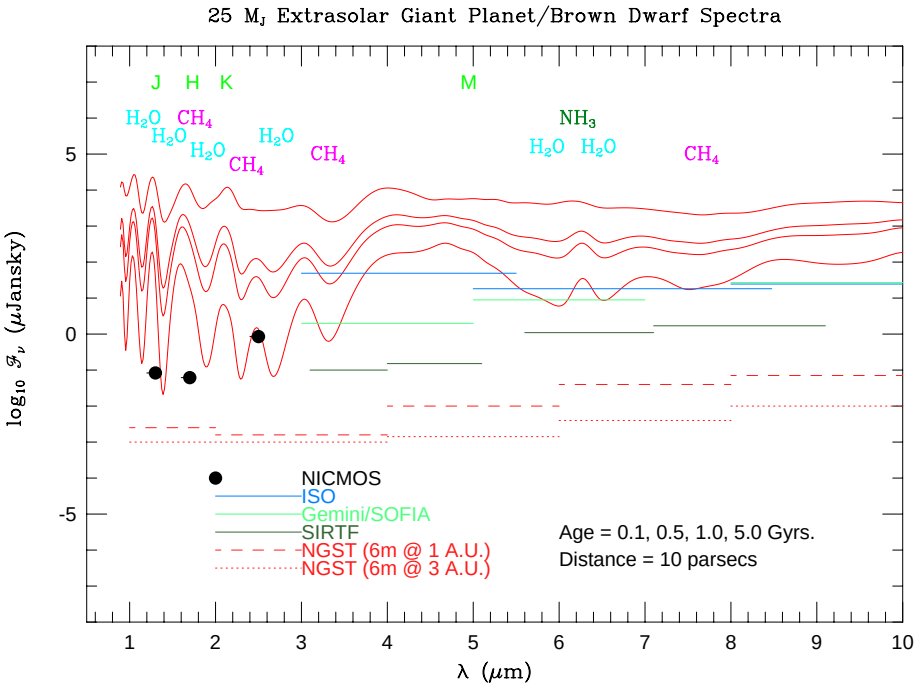

Figure 7. The flux (in μJanskys) at 10 parsecs versus wavelength (in microns) from 1 μm to 10 μm for a 25 M_J object at ages of 0.1, 0.5, 1.0, and 5.0 Gyr. Superposed are the positions of the J, H, K, and M bands, as well as the estimated sensitivities of the three NICMOS cameras, ISO, Gemini/SOFIA, SIRTF, and NGST.

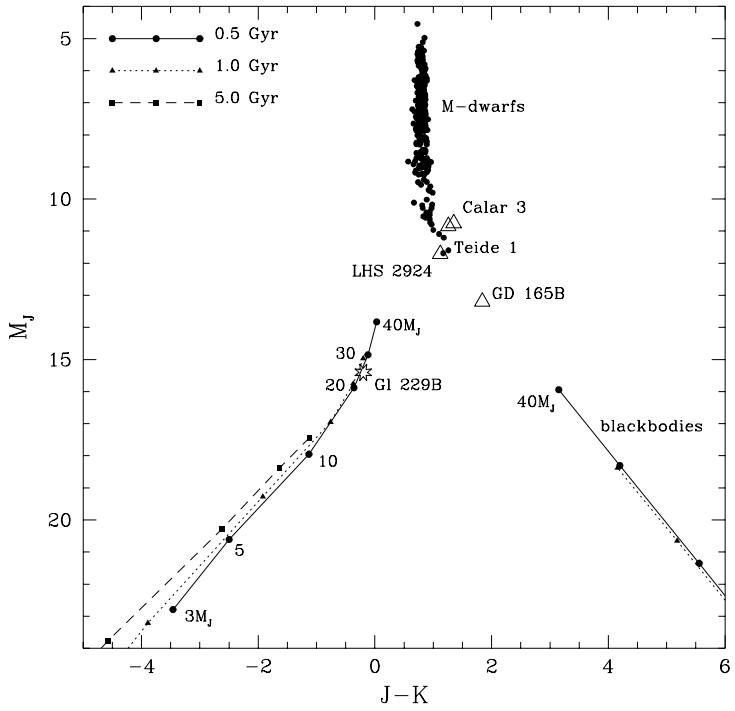

Figure 8. Absolute J vs. $J-K$ color–magnitude diagram. Theoretical isochrones are shown for $t = 0.5$, 1, and 5 Gyr, along with their black body counterparts. The difference between black body colors and model colors is striking. The brown dwarf, Gliese 229B (Oppenheimer *et al.* 1995), the young brown dwarf candidates Calar 3 and Teide 1 (Zapatero-Osorio, Rebolo, & Martin 1997), and late M dwarfs LHS 2924 and GD165B (Kirkpatrick, Henry, & Simons 1994,1995)) are plotted for comparison. The lower main sequence is defined by a selection of M–dwarf stars from Leggett (1992).

5. Infrared Colors

To calculate IR colors, we employed the transmission curves of Bessell & Brett (1988) and Bessell (1990) to define the photometric bandpasses and the model of Vega by Dreiling & Bell (1980) for the calibration of the magnitude scale. Figure 8 is a representative color–magnitude diagram for objects with masses from 3 $M_{\rm J}$ to 40 $M_{\rm J}$, for ages of 0.5, 1.0, and 5.0 Gyr. Figure 9 is a color–color diagram for the same models. Tables 4 & 5 depict the infrared magnitudes and colors for various combinations of mass and age. As Table 4 and Figure 8 suggest, the brightnesses in the near IR are quite respectable.

For comparison, included in these figures are the corresponding black body curves, hot, young brown dwarf or extremely late M dwarf candidates such as LHS2924, GD 165B, Calar 3, and Teide 1 (Kirkpatrick, Henry, & Simons 1994,1995; Zapatero-Osorio, Rebolo, & Martin 1997), and a sample of M dwarfs from Leggett (1992). These figures collectively illustrate the unique color realms occupied by extrasolar giant planets and brown dwarfs.

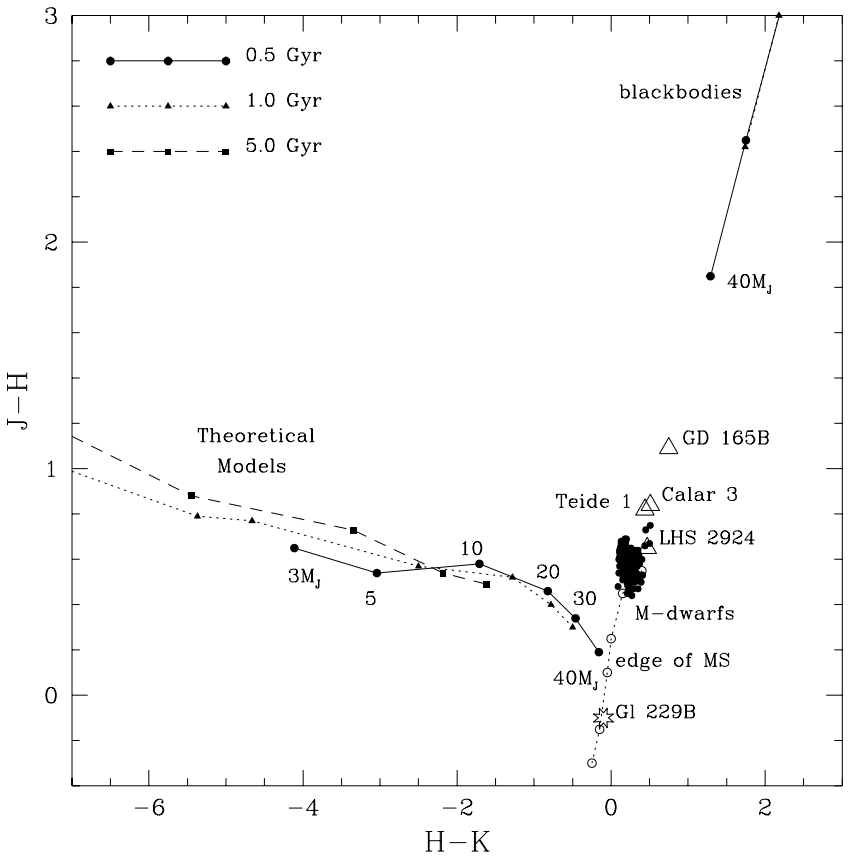

Figure 9. $J - H$ vs. $H - K$ color–color diagram. The edge of the main sequence as a function of metallicity, from our calculations employing Allard & Hauschildt (1995) atmosphere models, is shown for metallicities from [M/H]=0 (top) to [M/H]=–3 (bottom). Otherwise as in Figure 8.

Figure 8 portrays the fact that the J versus $J-K$ infrared H–R diagram loops back to the blue below the edge of the main sequence and is not a continuation of the M dwarf sequence into the red. For J versus $J-K$, the difference between the black body curves and the model curves is between 3 and 10 magnitudes. Gl229B fits nicely on these theoretical isochrones. The suppression of K by H_2 and CH_4 features is largely responsible for this anomalous blueward trend with decreasing mass and $T_{\rm eff}$. The fit to Gl229B in H is not as good. This is also true of the fit to L'. Since both H and L' have significant CH_4 features in them, we surmise that incompleteness or errors in the CH_4 opacity database is the cause. $J-H$ actually reddens with decreasing $T_{\rm eff}$, but only marginally and is still 1.5 to 4 magnitudes bluer than the corresponding black body. That the $J-H$ and $H-K$ colors of EGPs and brown dwarfs are many magnitudes blueward of black bodies is a firm result.

Table 4. Absolute Magnitudes of Synthetic BD/EGPs, [M/H]=0.0 †

Mass (M_J)	Age (Gyr)	M_J	M_H	M_K	$M_{L'}$	M_M	M_N
40	0.5	13.83	13.64	13.80	12.17	11.86	11.32
	1.0	14.97	14.67	15.17	13.06	12.41	12.25
	5.0	17.46	16.98	18.59	14.82	13.71	13.96
30	0.5	14.85	14.52	14.98	12.94	12.25	12.09
	1.0	15.75	15.35	16.13	13.62	12.73	12.77
	5.0	18.39	17.85	20.03	15.54	14.18	14.46
20	0.5	15.88	15.42	16.24	13.71	12.69	12.78
	1.0	16.95	16.43	17.71	14.51	13.28	13.51
	5.0	20.28	19.55	22.90	16.81	14.95	15.09
10	0.5	17.95	17.37	19.08	15.31	13.71	13.97
	1.0	19.27	18.70	21.19	16.27	14.41	14.59
	5.0	23.76	22.88	28.33	19.22	16.38	15.91
5	0.5	20.61	20.08	23.12	17.26	14.95	14.95
	1.0	23.21	22.43	27.09	18.86	15.94	15.62
	5.0	29.69	28.21	37.20	22.83	18.39	16.80
3	0.5	22.79	22.14	26.25	18.64	15.76	15.47
	1.0	24.82	24.02	29.40	19.92	16.58	15.93
	5.0	34.63	32.10	45.21	25.43	19.48	17.50

†We employed the transmission curves of Bessel & Brett (1988) and Bessel (1990) to define the photometric bandpass and the model of Vega by Dreiling & Bell (1980) for the calibration of the magnitude scale.

6. Conclusions and Future Work

Soon, planet and brown dwarf searches will be conducted by NICMOS, SIRTF, Gemini/SOFIA, ISO, NGST, LBT (Angel 1994), the MMT (Angel 1994), the VLT, Keck I & II, COROT (transits), DENIS, 2MASS, UKIRT, and IRTF, among other platforms. For close companions, advances in adaptive optics, interferometry, and coronagraphs will be necessary. The models we have generated

Table 5. Color Indices of Synthetic BD/EGPs, [M/H]=0.0 †

Mass (M_J)	Age (Gyr)	$J-H$	$J-K$	$H-K$	$K-L'$	$M-N$
40	0.5	0.19	0.03	-0.16	1.63	0.54
	1.0	0.30	-0.20	-0.50	2.11	0.16
	5.0	0.49	-1.13	-1.62	3.78	-0.25
30	0.5	0.34	-0.12	-0.46	2.04	0.17
	1.0	0.40	-0.38	-0.78	2.50	-0.04
	5.0	0.54	-1.64	-2.18	4.49	-0.28
20	0.5	0.46	-0.36	-0.82	2.54	-0.08
	1.0	0.52	-0.76	-1.28	3.20	-0.22
	5.0	0.73	-2.62	-3.35	6.09	-0.14
10	0.5	0.58	-1.13	-1.71	3.77	-0.26
	1.0	0.57	-1.93	-2.50	4.93	-0.18
	5.0	0.88	-4.57	-5.45	9.12	0.47
5	0.5	0.54	-2.50	-3.04	5.86	0.00
	1.0	0.77	-3.89	-4.66	8.24	0.32
	5.0	1.48	-7.51	-8.99	14.38	1.59
3	0.5	0.65	-3.46	-4.11	7.61	0.30
	1.0	0.79	-4.58	-5.37	9.47	0.65
	5.0	2.53	-10.58	-13.11	19.78	1.98

† We employed the transmission curves of Bessel & Brett (1988) and Bessel (1990) to define the photometric bandpass and the model of Vega by Dreiling & Bell (1980) for the calibration of the magnitude scale.

of the colors and spectra of EGPs and brown dwarfs are in aid of this quest. We have created a general non–gray theory of objects from 0.3 $M_{\rm J}$ to 70 $M_{\rm J}$ below $\sim$1300 K, but the opacity of CH_4 and a proper treatment of silicate/iron, H_2O, and NH_3 clouds are future challenges that must be met before the theory is complete. Since the near IR signature of nearby substellar companions will be significantly altered by a reflected component, a theory of albedos in the optical and in the near IR must be developed. In particular, it will be useful in the future to predict the signatures of specific systems with known orbital characteristics, primaries, and ages, such as τ Boo, 51 Peg, υ And, 55 Cnc, ρ CrB, 70 Vir, 16 Cyg, and 47 UMa.

It is rare that Nature conspires to make the objects of astronomical study easier to detect than simple estimates first imply. However, our calculations indicate that, whether they exist in profusion, or are merely a minority constituent of the solar neighborhood, EGPs and brown dwarfs might be detected and characterized with a bit more ease than originally feared.

Acknowledgments. We thank F. Allard, I. Baraffe, G. Chabrier, S. Kulkarni, J. Liebert, A. Nelson, B. Oppenheimer, and N. Woolf for a variety of useful contributions. This work was supported under NSF grants AST-9318970 and AST-9624878 and under NASA grants NAG5-2817, NAGW-2250, and NAG2-6007.

References

Allard, F., & Hauschildt, P.H. 1995, ApJ, 445, 433

Allard, F., Hauschildt, P.H., Baraffe, I., & Chabrier, G. 1996, ApJ, 465, L123

Allard, F., Hauschildt, P. H., Alexander, D. R. & Starrfield, S. 1997, ARA&A, 35, 137

Alexander, D. 1996, private communication

Angel, J.R.P. 1994, Nature, 368, 203

Benvenuti, P. *et al.* 1994, in *ESA's Report to the 30th COSPAR Meeting, ESA SP-1169, Paris*, p. 75 (ISO)

Borysow, A. & Frommhold, L. 1990, ApJ, 348, L41

Burrows, A., Hubbard, W.B., Saumon, D., & Lunine, J.I. 1993, ApJ, 406, 158

Burrows, A., Saumon, D., Guillot, T., Hubbard, W.B., & Lunine, J.I. 1995, Nature, 375, 299

Burrows, A., Marley, M., Hubbard, W.B., Lunine, J.I., Guillot, T., Saumon, D., Freedman, R., Sudarsky, D., & Sharp, C. 1997, submitted to Ap. J.

Bessell, M.S. 1990, PASP, 102, 1181

Bessell, M.S., & Brett, J.M. 1988, PASP, 100, 1134

Butler, R. P. & Marcy, G. W. 1996, ApJ, 464, L153

Butler, R. P., Marcy, G. W., Williams, E., Hauser, H., & Shirts, P. 1997, ApJ, 474, L115

Cochran, W.D., Hatzes, A.P., Butler, R.P., & Marcy, G. 1997, Science, in press

Dreiling, L.A. & Bell, R.A. 1980, ApJ, 241, 736

Eisenberg, D. & Kauzmann, W. 1969, The Structure and Properties of Water (New York: Oxford University Press)

Erickson, E. F. 1992, Space Science Reviews, 61, 61 (SOFIA)

Erickson, E. F. & Werner, M. W. 1992, Space Science Reviews, 61, 95 (SIRTF)

ExNPS: A Road Map for the Exploration of Neighboring Planetary Systems, JPL Publication 96–22, August 1996

Fegley, B. & Lodders, K. 1994, Icarus, 110, 117

Fegley, B. & Lodders, K. 1996, ApJ, 472, L37

Geballe, T. R., Kulkarni, S. R., Woodward, C. E., & Sloan, G. C. 1996, ApJ, 467, L101

Goody, R., West, R., Chen, L., & Crisp, D. 1989, J. Quant. Spectr. Rad. Transfer, 42, 539

Goorvitch, D. 1994, ApJS, 95, 535

Grossman, A.S. & Grant, K. 1992, LLNL Rept. UCRL-ID-111805

Grossman, A.S. & Grant, K. 1994a, LLNL Rept. UCRL-ID-116533

Grossman, A.S. & Grant, K. 1994b Eighth Conference on Atmospheric Radiation, 97, American Meterological Society.

Guillot, T., Burrows, A., Hubbard, W.B., Lunine, J.I., & Saumon, D. 1996, ApJ, 459, L35

Handbook of Chemistry and Physics, 74th Edition, 1993, ed. D.R. Lide, CRC Press Inc.

Husson, N., Bonnet, B., Scott, N.A., & Chedin, A. 1994, J. Quant. Spect. Rad. Transfer, 48, 509

ISO Observer's Manual Version 2.0, 31 March 1994, prepared by the ISO Science Operations Team, p6

Kirkpatrick, J.D., Henry, T.J., & Simons, D.A. 1994, AJ, 108, 1437

Kirkpatrick, J.D., Henry, T.J., & Simons, D.A. 1995, AJ, 109, 797

Kurucz, R.L., 1970, Smithsonian Obs. Spec. Rep., 309, 1-291

Lacis, A.A. & Oinas, V. 1991, J. Geophys. Res., 96, 9027

Lange's Handbook of Chemistry, 1979, ed. J.A. Dean, McGraw-Hill Book Company, New-York

Latham, D. W., Mazeh, T., Stefanik, R.P., Mayor, M., & Burki G. 1989, Nature, 339, 38

Leger, A., *et al.* 1993, Darwin Mission Concept, proposal to ESA

Leggett, S.K. 1992, ApJS, 82, 351

Marcy, G. W. & Butler, R. P. 1996, ApJ, 464, L147

Marley, M., Saumon, D., Guillot, T., Freedman, R.S., Hubbard, W.B., Burrows, A., & Lunine, J.I. 1996, Science, 272, 1919

Matthews, K., Nakajima, T., Kulkarni, S.R., & Oppenheimer, B.R. 1996, AJ, 112, 1678

Mayor, M. & Queloz, D. 1995, Nature, 378, 355

Mountain, M., R. Kurz, R., & Oschmann, J. 1994, in *The Gemini 8-m Telescope Projects, S.P.I.E. Proceedings on Advanced Technology Optical Telescopes V*, 2199, p. 41 (Gemini)

Nakajima, T., Oppenheimer, B.R., Kulkarni, S.R., Golimowski, D.A., Matthews, K., & Durrance, S.T. 1995, Nature, 378, 463

Oppenheimer, B.R., Kulkarni, S.R., Matthews, K., & Nakajima, T. 1995, Science, 270, 1478

Partridge, H. & Schwenke, D.W. 1997, J. Chem. Phys., 106, 4618

Rothman, L.S., Gamache, R.R., Tipping, R.H., Rinsland, C.P., Smith, M.A.H., Benner, D.C., Malathy Devi, V., Flaud, J.-M., Camy-Peyret, C., Perrin, A., Goldman, A., Massie, S.T., Brown, L.R., & Toth, R.A. 1992, J. Quant. Spect. Rad. Transfer, 48, 469.

Rothman, L.S., Wattson, R.B., Gamache, R.R., Goorvitch, D., Hawkins, R.L., Selby, J.E.A., Cambry-Peyret, C., Flaud, J.-M., Schroeder, J., & McCann, A. 1997, J. Quant. Spect. Rad. Transfer, submitted

Saumon, D., Bergeron, P., Lunine, J.I., Hubbard, W.B. & Burrows, A. 1994, ApJ, 424, 333

Saumon, D., Hubbard, W.B., Burrows, A., Guillot, T., Lunine, J.I., & Chabrier, G. 1996, ApJ, 460, 993

Saxner, M. & Gustafsson, B. 1984, A&A, 140, 334

Thompson, R. 1992, Space Science Reviews, 61, 69 (NICMOS)

Tipping, R. 1990, Report on Calculation of Spectroscopic Parameters for Diatomic Molecules of Atmospheric Interest, Univ. of Alabama Report, Dept. of Physics and Astronomy

TOPS: Toward Other Planetary Systems, NASA Solar System Exploration Division, Washington, D.C., 1992

Tsuji, T., Ohnaka, W., Aoki, W., & Nakajima, T. 1996, A&A, 308, L29

Tyuterev, Vl.G., Babikov, Yu.L., Tashkun, S.A., Perevalov, V.I., Nikitin, A., Champion, J.-P., Wegner, Ch., Pierre, C., Pierre, G., Hilico, J.-C., & Loete, M. 1994, J. Quant. Spect. Rad. Transfer, 52, 459

Wattson, R.B., and Rothman L.S. 1992, J. Quant. Spectr. Rad. Transfer, 48, 763

Zapatero-Osorio, M.R., Rebolo, R., & Martin, E.L. 1997, A&A, 317, 164

Zheng, C. & Borysow, A. 1995, Icarus, 113, 84